



UNIVERSITY OF LEEDS

This is a repository copy of *The effect of highly inhomogeneous biphasic properties on mechanical behaviour of articular cartilage*.

White Rose Research Online URL for this paper:
<https://eprints.whiterose.ac.uk/175797/>

Version: Accepted Version

Article:

Lin, W, Meng, Q orcid.org/0000-0002-6708-5585, Li, J et al. (2 more authors) (2021) The effect of highly inhomogeneous biphasic properties on mechanical behaviour of articular cartilage. *Computer Methods and Programs in Biomedicine*, 206. 106122. ISSN 0169-2607

<https://doi.org/10.1016/j.cmpb.2021.106122>

© 2021, Elsevier. This manuscript version is made available under the CC-BY-NC-ND 4.0 license <http://creativecommons.org/licenses/by-nc-nd/4.0/>.

Reuse

This article is distributed under the terms of the Creative Commons Attribution-NonCommercial-NoDerivs (CC BY-NC-ND) licence. This licence only allows you to download this work and share it with others as long as you credit the authors, but you can't change the article in any way or use it commercially. More information and the full terms of the licence here: <https://creativecommons.org/licenses/>

Takedown

If you consider content in White Rose Research Online to be in breach of UK law, please notify us by emailing eprints@whiterose.ac.uk including the URL of the record and the reason for the withdrawal request.



eprints@whiterose.ac.uk
<https://eprints.whiterose.ac.uk/>

The effect of highly inhomogeneous biphasic properties on mechanical behaviour of articular cartilage

Weijian Lin¹, Qingen Meng², Junyan Li³, Zhenxian Chen^{4*} and Zhongmin Jin^{1,2,3*}

¹State Key Laboratory for Manufacturing System Engineering, School of Mechanical Engineering, Xi'an Jiaotong University, 710054, Xi'an, Shaanxi, China

²Institute of Medical and Biological Engineering, School of Mechanical Engineering, University of Leeds, Leeds, LS2 9JT, United Kingdom

³Tribology Research Institute, School of Mechanical Engineering, Southwest Jiaotong University, 610031, Chengdu, Sichuan, China

⁴Key Laboratory of Road Construction Technology and Equipment (Ministry of Education), Chang'an University, 710064, Xi'an, Shaanxi, China

*Corresponding author:

Prof. Zhongmin Jin

State Key Laboratory for Manufacturing System Engineering, School of Mechanical Engineering,

Xi'an Jiaotong University,

Xi'an, Shaanxi, China

Email: zmjin@xjtu.edu.cn

Zhenxian Chen

School of Mechanical Engineering,

Chang'an University,

Xi'an, Shaanxi, China.

Email: zhenxian_chen@yeah.net

Abstract

Background and Objective: Investigating the biomechanics of cartilage could help to understand the unique load-bearing property of the cartilage and optimize the scaffold design in tissue-engineering. It is important to model the cartilage as a highly inhomogeneous fibril-reinforced biphasic material to represent its complex composition and structure. The depth-dependent and strain-dependent properties of the cartilage would also play an important role in its mechanical behaviour. However, the differences in representing the cartilage as a highly inhomogeneous model or as simplified models still remain unclear. Hence, in this study, a highly inhomogeneous fibril-reinforced biphasic cartilage model considering both the depth-dependent and strain-dependent properties was constructed; the effect of highly inhomogeneous properties on the mechanical behaviour of articular cartilage was investigated.

Methods: A finite element model of the cartilage was developed based on a flat-ended indentation test. Compressive forces were applied to four various inhomogeneous layered models through a porous indenter (Model 1: nine layers with strain-dependent permeability; Model 2: three layers with strain-dependent permeability; Model 3: single layer with strain-dependent permeability; Model 4: nine layers with constant permeability).

Results: Models 1 and 2 provided similar results with less than 3% difference in the peak effective stress, contact pressure, fluid pressure as well as fluid support ratio. However, Model 1 to Model 3 differed in stress and strain distribution patterns along depth over prolonged loads, which may provide an important

insight into the highly inhomogeneous depth-dependent properties of cartilage. In addition, Model 1 with strain-dependent permeability demonstrated an enhanced capability on fluid pressurisation as compared with Model 4 which had constant permeability.

Conclusions: A highly inhomogeneous fibril-reinforced biphasic model considering both depth-dependent and strain-dependent properties was developed in this study, in order to illustrate the effect of highly inhomogeneous properties on the mechanical behaviour of the articular cartilage. The number of layers in the models with depth-dependent properties should be selected according to the research question and clinical demands. The model with strain-dependent permeability offers an enhanced capability on fluid pressurisation. In future studies, the proposed model could be adopted in cell-models to provide more in-depth information or in tissue-engineering to optimize the depth-dependent scaffold structure.

Keywords

Finite element, articular cartilage, inhomogeneous, biphasic, strain-dependent, depth-dependent, layered model

1 **1. Introduction**

2 Articular cartilage (AC), the composite of collagens, proteoglycans and liquid [1], is a highly
3 inhomogeneous material. Material properties of AC have a marked impact on its biomechanics. The finite
4 element (FE) method has been widely adopted to study the biomechanics of AC, which could help to
5 understand the unique load-bearing and lubrication properties of AC, prevent or treat osteoarthritis as well
6 as optimize the scaffold design in tissue engineering [2-4].

7 In order to investigate the mechanical response of AC, various material models have been developed
8 in FE method. As the most widely adopted model, the isotropic elastic model is suitable to describe two
9 situations: 1) an instantaneous load applied to the cartilage when fluid diffusion is minimal; 2) a
10 prolonged load applied to the cartilage when the equilibrium stage is reached and fluid ceases to diffuse
11 [5]. According to the biphasic theory [6], the solid structure of the cartilage confines the fluid within its
12 pores. Because of the permeability, fluid diffusion and pressurisation, mechanical response of AC is
13 time-dependent. Further, the fibril-reinforced biphasic model was developed to consider fibre properties
14 within the cartilage [7-9]. In a study comparing the maximum principal stresses and strains within AC
15 among these three typical material models [10], it was suggested that the maximum principal stresses and
16 strains predicted by simplified materials (isotropic elastic and biphasic) differed from the results of the
17 fibril-reinforced biphasic material [10]. In recent years, a more detailed cell-level model was proposed,
18 combining fibril-reinforced biphasic tissue and chondrocytes through a multiscale approach [8]. It was

19 suggested that deformation of the cell was influenced by the different tissue properties between the
20 samples and inhomogeneous properties within the sample. However, in this model, Young's modulus and
21 Poisson's ratio of AC were homogeneous, which might neglect the importance of depth-dependent
22 Young's modulus and Poisson's ratio of AC.

23 Due to the complex composition and structure of the cartilage, the properties of AC are
24 depth-dependent and strain-dependent [11, 12]. For example, the Young's modulus, Poisson's ratio, water
25 volume fraction, fibrillar direction and permeability of AC vary across the depth of AC [12, 13]. The
26 depth-dependent properties are usually characterised by three zones - the surface, the middle and the deep
27 zones respectively account for 10-20%, 40-60% and almost 30% of the whole thickness [14]. Meanwhile,
28 the permeability of AC is shown to be strain-dependent [11, 15], which is mainly induced by finite
29 compression [16]. Additionally, the permeability is influenced by the orientation of fibres and the torsion
30 of tissue [17]. It was reported that the fluid diffusion is higher along the direction parallel to the fibre than
31 the other directions [18, 19], and the torsion of tissue would create a helical flow pattern [17]. This study
32 suggested that the depth-dependent and strain-dependent properties may have significant effect on the
33 mechanical behaviour of AC. However, the depth-dependent and strain-dependent properties of cartilage
34 have been usually neglected in most of the previous FE studies [8, 20, 21].

35 As for the depth-dependent properties, some studies adopted a three-layered model. When compared
36 with a homogeneous model, a three-layered model could provide a higher radial strain in the deep zone

37 and a highly heterogeneous stress distribution [22]. Such relatively high strain and stress in local areas
38 may be the reason for tissue fibrillation or delamination [22, 23]. Another three-layered model
39 considering osmotic pressure, fluid diffusion, chemical expansion and depth-dependent properties was
40 developed to study the relevance of inhomogeneous properties in the mechanical behaviour of AC [24].
41 However, this study [25] suggested that three-layered model may not be accurate enough to predict the
42 stress and pressure along depth of AC and hence a highly inhomogeneous model (more than three layers)
43 may be needed. A previous study [12] suggested that the cartilage could be divided into nine layers, which
44 may provide more precise biomechanical information. They found out that the depth-dependent
45 compressive modulus in nine layers would significantly affect the biomechanics of cartilage (e.g. strains
46 distribution). Moreover, investigation of the highly inhomogeneous depth-dependent properties could
47 contribute to tissue-engineering. According to recent reviews [3], there is a great demand to construct the
48 depth-dependent scaffold model in tissue-engineering functional cartilage but it is still challenging at this
49 moment. Currently, few studies have adopted the highly inhomogeneous depth-dependent properties in
50 multi-layered model (more than three layers). The differences between this multi-layered model and
51 simplified models (three-layered and single-layered) remain unclear.

52 As for the permeability, constant permeability and strain-dependent permeability are most widely
53 adopted. Some FE studies adopted the constant permeability to simplify the material properties. For
54 example, constant permeability was widely assumed in biphasic models [26, 27]. Recently, more and

55 more FE studies [8, 16] started to consider the strain-dependent permeability based on experiments [11].
56 However, to the best of our knowledge, no study has quantified the difference between FE models
57 adopting constant permeability and strain-dependent permeability.

58 Therefore, this study aims to 1) propose a highly inhomogeneous fibril-reinforced biphasic model
59 considering both depth-dependent (Young's modulus, Poisson's ratio, water volume fraction, fibrillar
60 direction and permeability) and strain-dependent (permeability) properties; 2) investigate the effect of
61 highly inhomogeneous properties on the mechanical behaviour of AC by comparing four different FE
62 models (Model 1: nine layers with strain-dependent permeability; Model 2: three layers with
63 strain-dependent permeability; Model 3: single layer with strain-dependent permeability; Model 4: nine
64 layers with constant permeability). The rest of the paper is organized as follows: Section 2 defines the
65 indentation experiment and the highly inhomogeneous material, followed by constructing four FE models;
66 Section 3 presents the simulation results; Section 4 discusses two aspects including 1) the comparison
67 between models with different number of layers; 2) the comparison between models with
68 strain-dependent permeability and constant permeability; Section 5 concludes the paper.

69 **2. Materials and Methods**

70 **2.1 FE model**

71 The FE model of the cartilage introduced in this study was developed based on the widely used
72 porous flat-ended indentation test [28]. According to a previous study [29], the size effect of the cartilage

73 could be neglected if the radius of cartilage was modelled four times larger than the radius of the indenter.

74 Thus, the cartilage ($R = 5 \text{ mm}$, $h = 1.125 \text{ mm}$) was indented by a porous flat-ended indenter ($R_{\text{ind}} = 1 \text{ mm}$)

75 in our study (Figure 1(a)) [30]. The forces applied to the top of the indenter were ramped over 12 s and

76 held constant for 4000 s. Two loading scenarios were analysed in this study. In order to verify the model,

77 a 0.35 N force was adopted based on a previous experiment [30]. In order to better compare the predicted

78 results among different material models under physiological loads, a 1.20 N force was analysed to

79 simulate the large deformation of the cartilage within the joint during daily activity [31]. To reduce the

80 computational cost, a quarter of the symmetric model was adopted. Then the model was divided into nine

81 layers of the same thickness (Figure 1(b)) and represented by about 43,500 hexahedral elements. The

82 choice of nine layers and the thickness of each layers ($125 \mu\text{m}$) are based on previous experiments [12],

83 which allows assessment of the cartilage deformation over length scale much greater than that of the

84 in-dwelling cell (diameter 5-15 μm) in experiments [32]. The mesh convergence study on the density of

85 element was carried out. The changes in peak fluid pressure and contact pressure were less than 5% by

86 doubling the number of elements. The bottom of the cylindrical cartilage was fully constrained and

87 modelled as an impermeable surface based on experiments [19]. Free-draining boundary condition was

88 set at the top and lateral surfaces of cartilage [29].

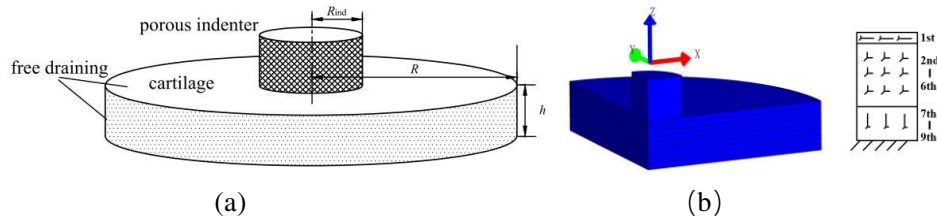


Figure 1. The porous flat-ended indentation test: schematic plot (a); A quarter of symmetric model and depth-dependent fibrillar distributions pattern (b)

The fibril-reinforced biphasic model constructed in the present study is based on two assumptions.

Firstly, we assumed that the ion concentration within AC remained constant (i.e. the Donnan osmotic pressure was constant), as the Donnan osmotic pressure is incorporated into the total stiffness of the solid-matrix in biphasic theory [33]. In addition, the strain causing by tissue swelling was relatively low when compared with the tissue strain under a physiological load [34, 35]. Secondly, the time-dependent behaviour of AC is dominated by biphasic mechanism and the flow-independent viscoelasticity of AC is not considered [36], as experimental results show that in all cartilage zones, the mechanical behaviour can be better described by the nonlinear biphasic model than viscoelastic model [37].

The fibrillar distribution pattern of AC is based on our previous study [21]. Fibres were assumed parallel to the cartilage surface in the surface zone and perpendicular to the cartilage surface in the deep zone; while in the middle zone, fibres were randomly distributed [38]. In our models (Figure 1(b)), the primary fibres were parallel to the articular surface (x-direction) in the 1st layer of elements and perpendicular to the cartilage surface (z-direction) in the 7th-9th layers, and the other two secondary fibres were orthogonal to the direction of the primary fibres. In the primary direction, the effective tensile

107 modulus of fibres was 6 MPa. Meanwhile, 2 MPa was adopted for the other two orthogonal directions of
108 fibres. In the 2nd-6th layers, the fibres were equally distributed in three directions to simulate the
109 randomly distributed fibres in the middle zone of AC, and the effective tensile modulus of the fibres was
110 3 MPa.

111 The strain energy function of the fibre [39, 40] was formulated by

$$112 \quad \Psi = \frac{\xi}{\alpha\beta} \left(\exp[\alpha(I_n - 1)^\beta] - 1 \right) \quad (1)$$

113 where α and β are the coefficient and the power of exponential argument, respectively; ξ is the
114 measure of the fibrillar modulus (one-quarter of the effective tensile modulus of fibre) and I_n is the
115 square of the fibre stretch.

116 Eq.(1) produced a power law when $\alpha \rightarrow 0$,

$$117 \quad \lim_{\alpha \rightarrow 0} \Psi = \frac{\xi}{\beta} (I_n - 1)^\beta \quad (2)$$

118 The fibre only sustains tension and does not provide any resistance in compression situation.
119 Therefore, $\alpha \rightarrow 0$ and $\beta = 2$ were adopted to convert the stress from compression to tension
120 discontinuously in this study. The effect of different fibrillar distribution pattern has been studied and
121 discussed in our previous studies [20, 21]. Therefore, only the depth-dependent non-fibrillar properties
122 were discussed in the present study.

123 The depth-dependent parameters of cartilage were set according to previous studies [12, 13, 19]. The
124 depth-dependent equilibrium compressive modulus, Poisson's ratio were calculated from Eq. (3). These

125 two parameters were defined as [13]:

$$126 \quad E = E_m \left(1 + \frac{\alpha_E z}{h} \right), \nu = \nu_m \left(1 + \frac{\alpha_\nu z}{h} \right) \quad (3)$$

127 where E_m is Young's modulus and ν_m is Poisson's ratio at the cartilage surface; z and h represent
 128 the depth from the cartilage surface and the thickness of the cartilage, respectively; α_E and α_ν are
 129 constants. In this study, the parameters ($E_m = 0.53$ MPa, $\nu_m = 0.12$, $\alpha_E = 3.2$ and $\alpha_\nu = 2.8$) were adopted
 130 based on previous studies [13, 37].

131 The depth-dependent fluid volume fraction φ_f was defined as follows [41]:

$$132 \quad \varphi_f = 0.9 - 0.2 \frac{z}{h} \quad (4)$$

133 According to the experiments of Maroudas [19], the depth-dependent permeability was assumed to
 134 increase from the surface to the middle of cartilage, and decrease in the deep layer of the cartilage. The
 135 depth-dependent, strain-dependent and anisotropic (induced by the orientation of fibres and finite torsion
 136 of the cartilage) permeability of cartilage changes exponentially as formulated [13, 15, 17, 40, 42]:

$$137 \quad \mathbf{k} = \sum_{a=1}^3 k_a \mathbf{m}_a \quad (5)$$

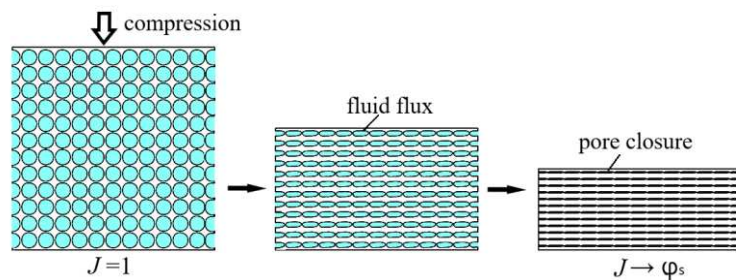
138 where k_a are the current permeability and \mathbf{m}_a are second order tensors denoting the spatial structural
 139 tensors that describe the orthogonal planes of symmetry. k_a and \mathbf{m}_a are formulated as follows:

$$140 \quad \left\{ \begin{array}{l} k_a(J) = \frac{k_{a0}}{J^2} \left(\frac{J - \varphi_s}{1 - \varphi_s} \right)^{\alpha_c} e^{\frac{1}{2} M (J^2 - 1)} \\ k_{a0} = \left[1 + 4.3 \frac{z}{h} - 7.8 \left(\frac{z}{h} \right)^2 + 3.1 \left(\frac{z}{h} \right)^3 \right] k_m \end{array} \right., a = 1, 2, 3 \quad (6)$$

141 $\mathbf{m}_a = \mathbf{F} \cdot (\mathbf{V}_a \otimes \mathbf{V}_a) \cdot \mathbf{F}^T$ (7)

142 where J is the relative volume of the cartilage (the current volume was divided by the initial volume); k_{a0}
 143 is the initial permeability in the original state ($a=1, 2, 3$ represent x, y, z direction, respectively); k_m is
 144 the permeability at the cartilage surface, which was set to $0.9 \times 10^{-3} \text{ mm}^4/\text{N s}$ in this study [25, 43]; φ_s
 145 is the solid volume fraction of the cartilage; M and α_e are the exponential strain-dependent constant and
 146 power-law exponent respectively; \mathbf{F} is the deformation gradient; \mathbf{V}_a are orthonormal vectors normal to the
 147 planes of symmetry.

148 To further explain the strain-dependent permeability, the process of pore closure is illustrated in
 149 Figure 2. The pore closure would occur as relative volume is reduced to the solid volume fraction φ_s ,
 150 which also means the permeability $k_a(J)$ reduces to 0, and the fluid inside the cartilage would not 'squeeze
 151 out'. On the one hand, if M and α_e were set to zero, Eq.(6) collapsed to a constant permeability. On the
 152 other hand, when $M = 4.638$ and $\alpha_e = 0.0848$ were chosen based on the previous experiment [15], a
 153 strain-dependent permeability was produced in this study.



154
 155 Figure 2. The process of pore closure in biphasic material under compression: the pore closure occurs
 156 when the relative volume J (the current volume was divided by the initial volume) is reduced to the solid
 157 volume fraction φ_s under the compression load.

158 In the present study, the permeability along the direction parallel to the fibres was assumed twice as
159 much as that along the direction perpendicular to the fibres [18, 25]. Based on the equations and
160 parameters illustrated above, the depth-dependent and strain-dependent parameters were determined.

161 The non-fibrillar solid-matrix of the cartilage was represented as *neo-Hookean* material in FEBio. Its
162 hyperelastic strain-energy function (W) [40] was defined as

$$163 \quad W = \frac{\mu}{2}(I_1 - 3) - \mu \ln J + \frac{\lambda}{2}(\ln J)^2 \quad (8)$$

164 where I_1 is the first invariants of the right Cauchy-Green deformation tensor; μ and λ are the
165 Lamé parameters, which can be determined by Young's modulus and Poisson's ratio

$$166 \quad \lambda = \frac{\nu E}{(1+\nu)(1-2\nu)}, \mu = \frac{E}{2(1+\nu)} \quad (9)$$

167 The porous indenter was modelled as a biphasic isotropic elastic material with a sufficiently large
168 Young's modulus $E = 1,000$ MPa. Other properties were set as follows: $\nu = 0.3$, $\phi_s = 0.8$, $k = 10$ mm⁴ / N s.

169 All the analyses were carried out in a finite element solver FEBio (Version 2.9, www.febio.org) [44].

170 The FEBio implementation considers free-draining boundary condition at the non-contact area and
171 enforce the continuity of the fluid flux as well as contact traction across the contact surfaces
172 simultaneously. By contrast, this free-draining boundary condition should be modified by additional
173 user-developed subroutines in ABAQUS [2, 9, 45]. In our model, fluid was allowed to flow from one side
174 of the cartilage surface to the surface of the indenter. The contact between indenter and cartilage was set
175 to be frictionless. In order to enforce the contact constraint, the penalty method was chosen and a proper

176 penalty parameter was calculated by the auto-penalty algorithm. Finally, three convergence criteria (i.e.
 177 displacement, energy and fluid pressure tolerance) were used to ensure the convergence of a time step.

178 2.2 Parametric analyses

179 The afore-proposed model was denoted as Model 1, which was a nine-layered model with the most
 180 comprehensive material properties including all the depth-dependent and strain-dependent parameters
 181 illustrated above. In order to study the effect of the depth-dependent and strain-dependent properties on
 182 the mechanical behaviour of AC, three other models with different material properties were constructed.
 183 To investigate the effect of depth-dependent properties, three-layered and single-layered models were
 184 constructed as Models 2 and 3, respectively. To study the importance of the strain-dependent permeability,
 185 the constant permeability was assumed in Model 4 ($M = 0$, $\alpha_e = 0$, referring to Eq. (6)). The parameters
 186 adopted in these four models are shown in Table 1. To prove that nine-layered model was adequate, an
 187 eighteen-layered model was also constructed. The total solution-time of eighteen-layered model was
 188 almost tripled while improvement of simulation accuracy was limited (less than 4% difference in the
 189 parameters of interest). Therefore, the nine-layered model was adopted as the gold standard model.

| | | 1st | 2nd | 3rd | 4th | 5th | 6th | 7th | 8th | 9th |
|---------------------------------|-------------|------|------|------|------|------|------|------|------|------|
| Model 1 (9 strain-dependent) | E | 0.62 | 0.81 | 1.00 | 1.19 | 1.38 | 1.57 | 1.75 | 1.94 | 2.13 |
| | ν | 0.14 | 0.18 | 0.21 | 0.25 | 0.29 | 0.33 | 0.36 | 0.40 | 0.44 |
| | φ_s | 0.11 | 0.13 | 0.16 | 0.18 | 0.20 | 0.22 | 0.24 | 0.27 | 0.29 |
| | k_{10} | 1.09 | 1.36 | 1.49 | 1.51 | 1.43 | 1.28 | 0.54 | 0.43 | 0.32 |
| | k_{20} | 0.55 | 1.36 | 1.49 | 1.51 | 1.43 | 1.28 | 0.54 | 0.43 | 0.32 |
| | k_{30} | 0.55 | 1.36 | 1.49 | 1.51 | 1.43 | 1.28 | 1.08 | 0.86 | 0.64 |

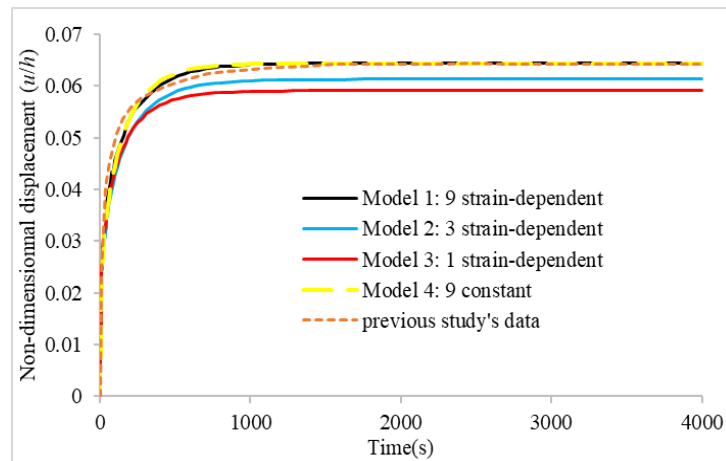
| | | | | | | | | | | | |
|---------------------------------|---------------|----------------------------|------|------|------|------|------|------|------|------|--|
| | M, α_e | $M=4.638, \alpha_e=0.0848$ | | | | | | | | | |
| Model 2 (3 strain-dependent) | E | 0.62 | | | 1.19 | | | | 1.94 | | |
| | ν | 0.14 | | | 0.25 | | | | 0.40 | | |
| | φ_s | 0.11 | | | 0.18 | | | | 0.27 | | |
| | k_{10} | 1.09 | | | 1.51 | | | | 0.43 | | |
| | k_{20} | 0.55 | | | 1.51 | | | | 0.43 | | |
| | k_{30} | 0.55 | | | 1.51 | | | | 0.86 | | |
| | M, α_e | $M=4.638, \alpha_e=0.0848$ | | | | | | | | | |
| Model 3 (1 strain-dependent) | E | 1.19 | | | | | | | | | |
| | ν | 0.25 | | | | | | | | | |
| | φ_s | 0.18 | | | | | | | | | |
| | k_{10} | 1.51 | | | | | | | | | |
| | k_{20} | 1.51 | | | | | | | | | |
| | k_{30} | 1.51 | | | | | | | | | |
| | M, α_e | $M=4.638, \alpha_e=0.0848$ | | | | | | | | | |
| Model 4 (9 constant) | E | 0.62 | 0.81 | 1.00 | 1.19 | 1.38 | 1.57 | 1.75 | 1.94 | 2.13 | |
| | ν | 0.14 | 0.18 | 0.21 | 0.25 | 0.29 | 0.33 | 0.36 | 0.40 | 0.44 | |
| | φ_s | 0.11 | 0.13 | 0.16 | 0.18 | 0.20 | 0.22 | 0.24 | 0.27 | 0.29 | |
| | k_{10} | 1.09 | 1.36 | 1.49 | 1.51 | 1.43 | 1.28 | 0.54 | 0.43 | 0.32 | |
| | k_{20} | 0.55 | 1.36 | 1.49 | 1.51 | 1.43 | 1.28 | 0.54 | 0.43 | 0.32 | |
| | k_{30} | 0.55 | 1.36 | 1.49 | 1.51 | 1.43 | 1.28 | 1.08 | 0.86 | 0.64 | |
| | M, α_e | $M=0, \alpha_e=0$ | | | | | | | | | |

190 Table 1. Material properties for every layer in all models. E : Young's modulus (MPa); ν : Poisson's ratio; φ_s :
191 solid volume fraction; k_{10}, k_{20}, k_{30} : the initial permeability in the x, y, z direction, respectively (10^{-3}
192 $\text{mm}^4/\text{N s}$); M and α_e : strain-dependence constants.

193 The parameters analysed include creep displacement, fluid pressure, contact pressure, total fluid flux,
194 relative permeability and fluid support ratio (the load supported by fluid divided by the total load). Other
195 mechanical outputs such as effective stress (i.e. Von Mises Stress) and z-strain (i.e. compressive strain)
196 were also recorded to make comparisons among these models. The analysis of these results may help to
197 understand the biomechanical behaviour of AC under compression.

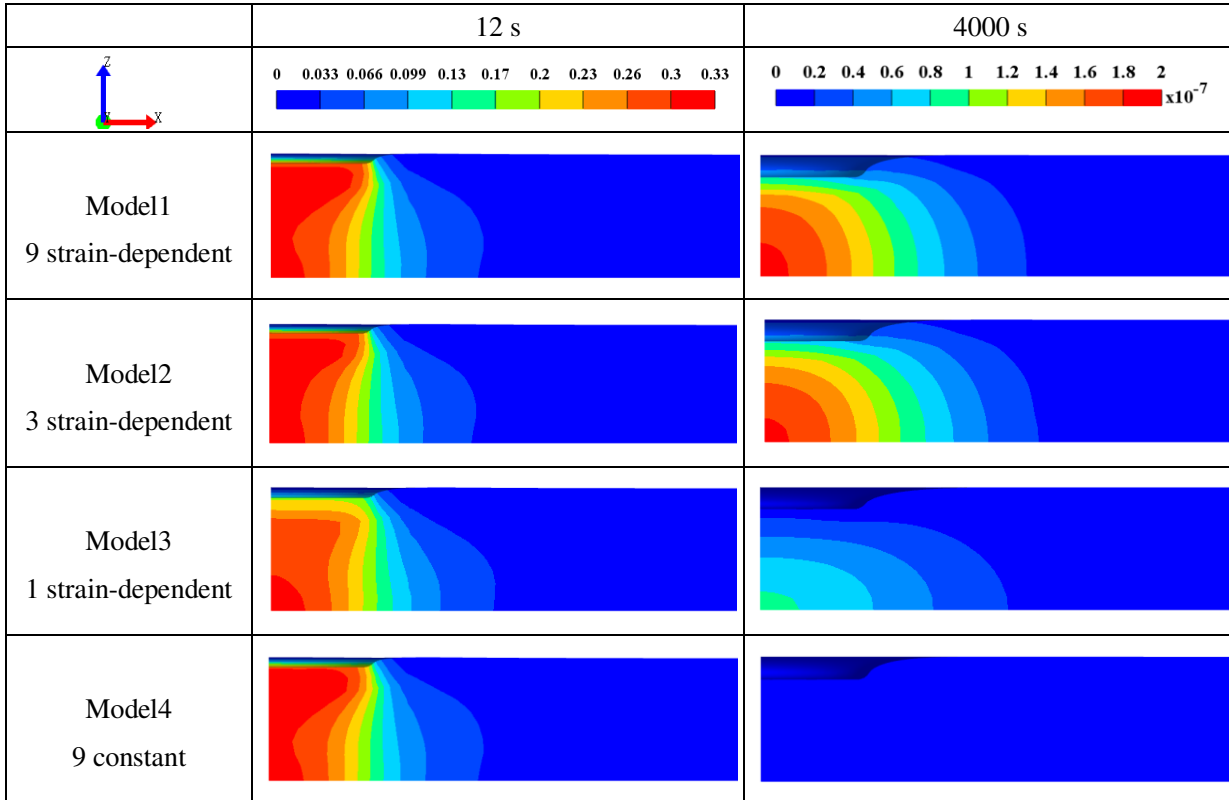
198 **3. Results**

199 Comparison of non-dimensional displacement of the indenter of the four FE models and previous
200 study's data under 0.35 N load is shown in Figure 3. Models 2 and 3 provided slightly smaller
201 displacements than previous study's data. Model 1 and Model 4 agreed with the previous study's data
202 well.



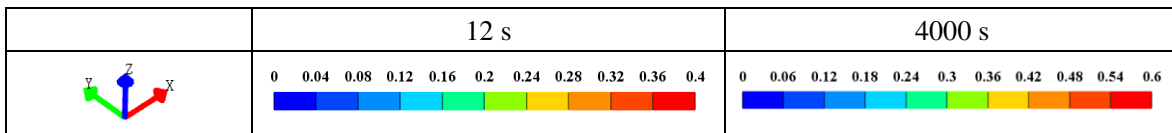
203 Figure 3. Non-dimensional creep displacement of the constructed models (Model 1 to Model 4) and
204 previous study's data: results over 4000 s period (u is the displacement of the indenter; h is the thickness
205 of the cartilage)
206

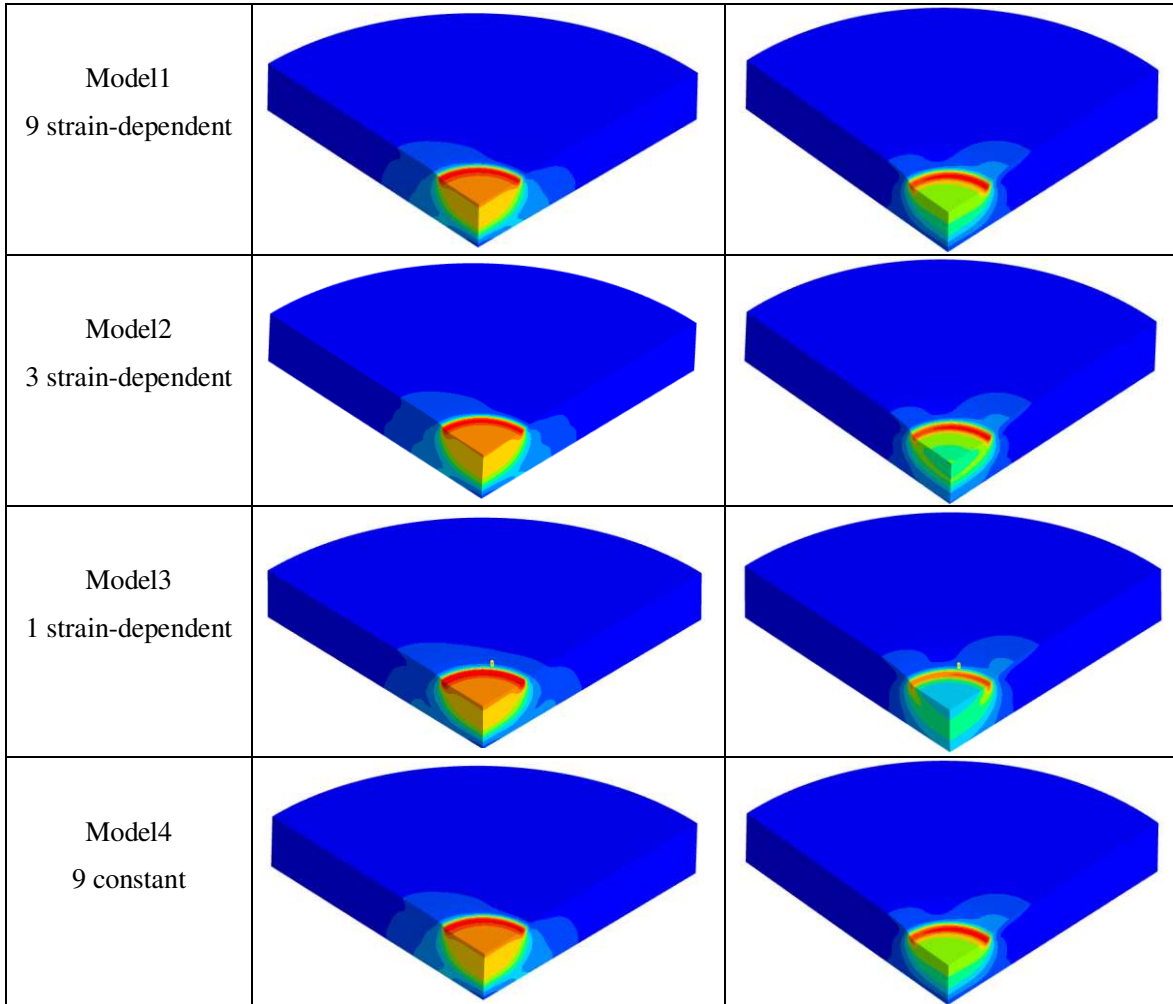
207 The contour of the fluid pressure for four models under a 1.20 N force at 12 s and 4000 s are shown
208 in Figure 4. In all models, the peak fluid pressure was found at the centre of the cartilage located below
209 the indenter. Model 3 had the lowest peak fluid pressure at 12 s. A similar fluid pressure pattern could be
210 observed in Model 1, Model 2 and Model 4 at 12 s. However, the fluid pressure of Model 4 decreased
211 markedly to nearly zero at 4000 s, while the decrease in fluid pressure of Model 1 and Model 2 was
212 slower than Model 4.



213 Figure 4. Contours of fluid pressure (MPa) of the cartilage in Models 1 to 4 at 12 s (left column) and 4000
 214 s (right column)

215 The distribution of the effective stress at the time of 12 s and 4000 s under a 1.20 N force are
 216 presented in Figure 5. The peak effective stress of Model 1, Model 2 and Model 4 were almost the same
 217 at both 12 s and 4000 s. At the time of 12 s, highest peak effective stress could be observed in Model 3,
 218 while lowest value in Model 3 occurred at 4000 s.

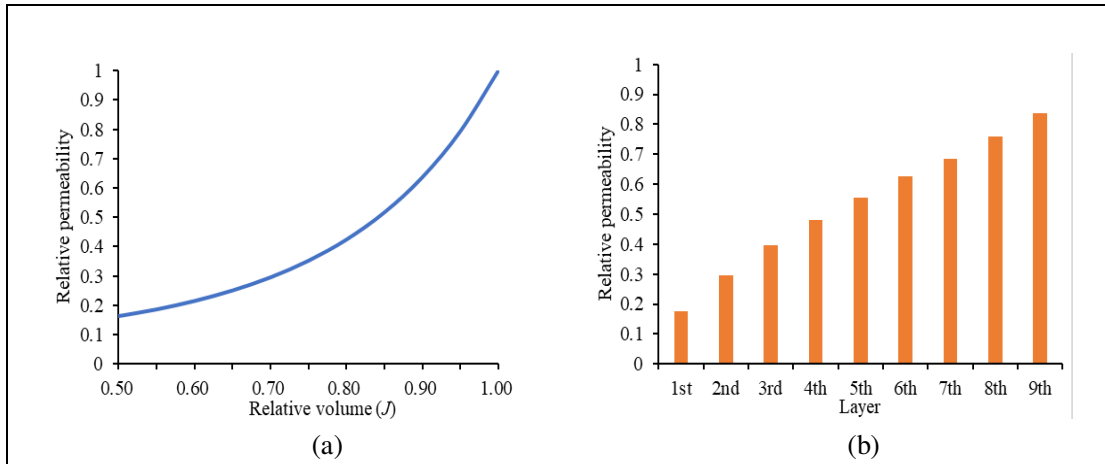




219 Figure 5. Contours of effective stress (MPa) of the cartilage in Models 1 to 4 at 12 s (left column) and
 220 4000 s (right column)

221 As shown in Figure 6, the relative permeability (current permeability divided by initial permeability)
 222 in Model 1 at the time of 4000 s under a 1.20 N force was calculated. The change of the relative
 223 permeability in the first layer of the cartilage is shown in Figure 6(a). When the relative volume reduced
 224 to 50% at the large deformation area, the permeability was less than 20% of the initial permeability. The
 225 minimum relative permeability in every layer is shown in Figure 6(b). The relative permeability was

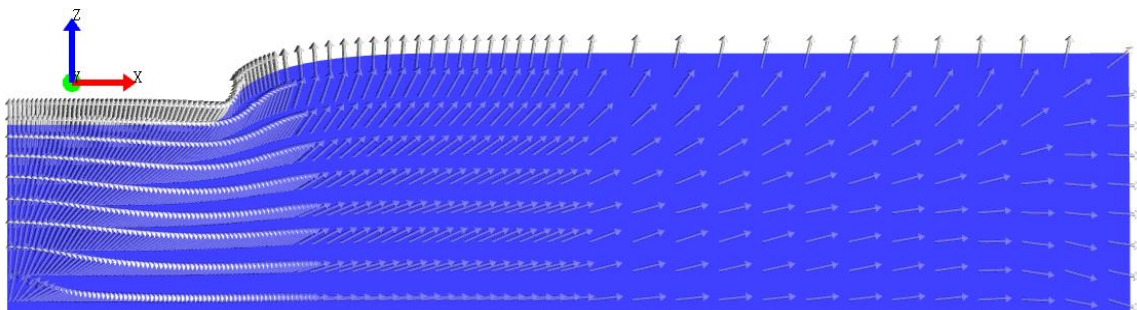
226 lowest in the surface zone and increased with the depth of the cartilage.



227 Figure 6. The variation in relative permeability (current permeability was divided by initial permeability)
228 with respect to the change of relative volume in the 1st layer (a); the minimum relative permeability in
229 every layer (b): at the instant of 4000 s in Model 1

230 The schematic plot of fluid flux and fluid diffusion direction inside the cartilage (grey arrows) is
231 presented in Figure 7. At the time of 4000 s, the fluid diffused from the bottom to the top and lateral
232 surfaces of cartilage. Moreover, the directions of fluid diffusion were influenced by the deformation and
233 torsion of the cartilage. No fluid flowed through the bottom of the cartilage due to the imposed
234 impermeable surface condition [19]. In order to visualise the fluid diffusion inside the cartilage, the
235 transparency of the cartilage was set from 1.0 to 0.5.

236



237 Figure 7. The schematic plot of fluid diffusion within the cartilage in x-z plane at the time of 4000 s

238 The predicted effective stress and z-strain of Model 1 to Model 3 along depth at the centre of the

239 cartilage are presented in Figure 8. At the time of 12 s, the effective stress and z-strain of three models

240 showed similar results: the surface zone of cartilage had larger stress and strain than those of the deep

241 zone. However, variances were observed at the time of 4000s s. Model 1 showed a relatively smoothly

242 gradient pattern along depth, Model 2 showed an obviously zonal pattern and Model 3 presented a

243 relatively even result.

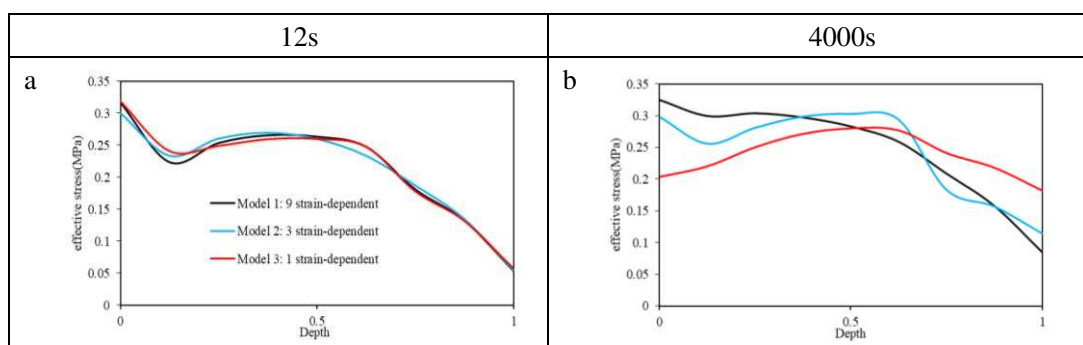
244 Fluid support ratios of Model 1 to Model 3 are presented in Figure 9. In order to better present the

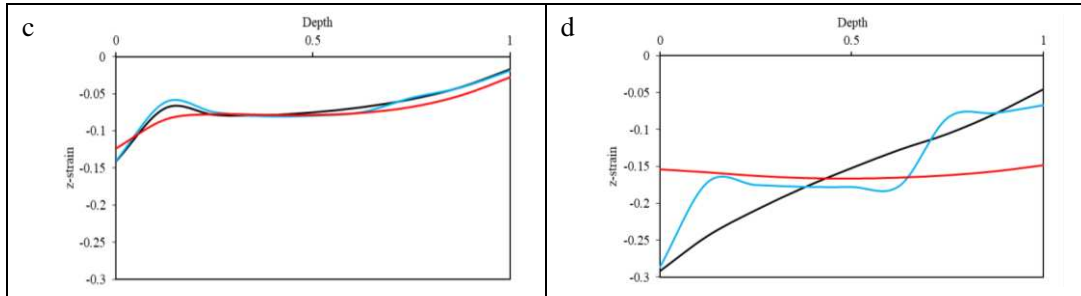
245 differences, only the results over 1000 s were shown. The fluid support ratios of Model 1 and Model 2

246 both reached 90% at the beginning of the simulations and gradually decreased to nearly zero over time.

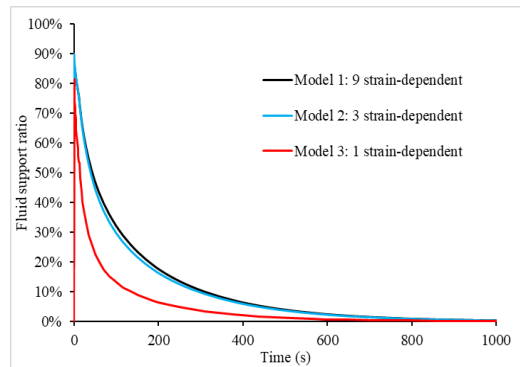
247 However, the peak fluid support ratio of Model 3 was only 82%, and its decreasing speed was much faster

248 when compared with those of Models 1 and 2.



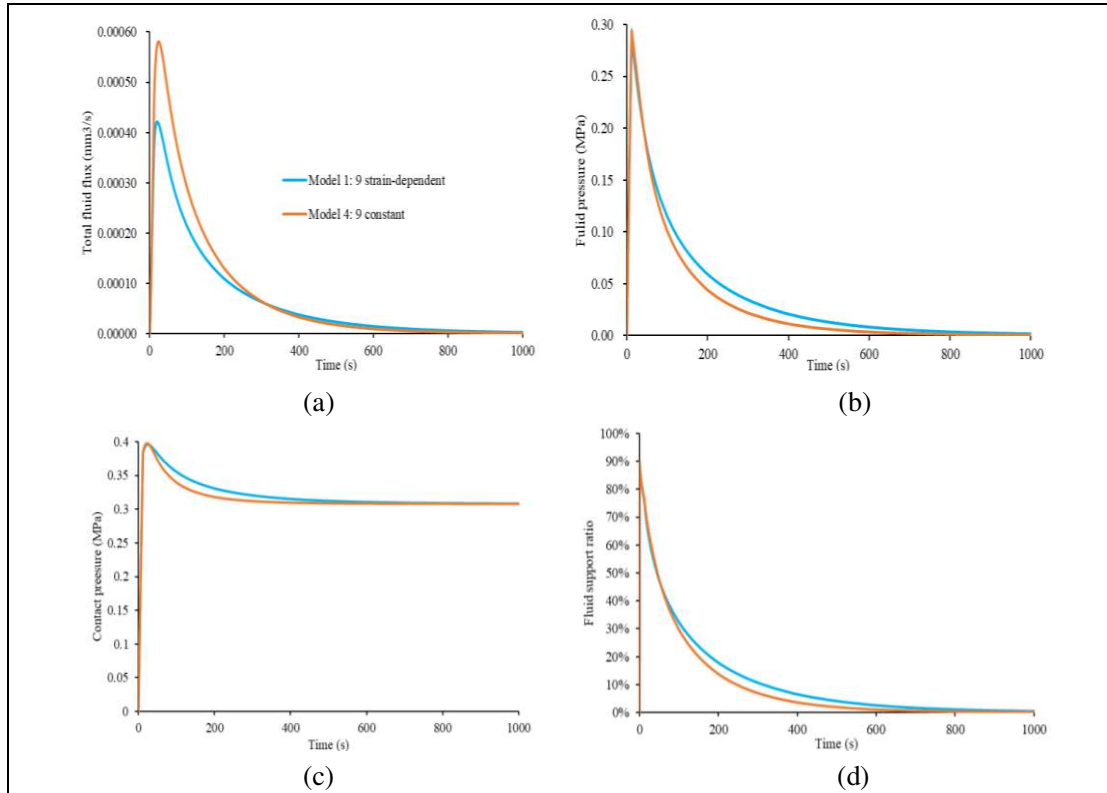


249 Figure 8. The effective stress and z-strain of Models 1 to Model 3 at different relative depth at the centre
 250 of the cartilage (0 represents the surface and 1 represents the bottom): at the time of 12 s (left column)
 251 and 4000 s (right column)



252
 253 Figure 9. The fluid support ratios of Model 1 to Model 3 over 1000 s period

254 The predicted total fluid flux, fluid pressure, contact pressure and fluid support ratio of Model 1 and
 255 Model 4 show obvious differences over time in Figure 10. To better present the differences, only the
 256 results over 1000 s are shown. The peak total fluid flux on the cartilage surface centre in Model 1 was
 257 almost two thirds of the total fluid flux in Model 4 (Figure 10(a)). The peak fluid pressure, peak contact
 258 pressure and peak fluid support ratio at the surface of cartilage in Model 1 and Model 4 were almost the
 259 same, but the results of Model 4 always decreased faster than those of Model 1 (Figure 10(b)-(d)).



260 Figure 10. Total fluid flux (at the surface of the cartilage) (a); Fluid pressure (at the surface of the
 261 cartilage) (b); Contact pressure (at the surface of the cartilage) (c); Fluid support ratio (d): results over
 262 1000 s period for the cartilage in Model 1 and Model 4

263 **4. Discussion**

264 In this study, a highly inhomogeneous fibril-reinforced biphasic model (Model 1) with
 265 depth-dependent and strain-dependent properties (e.g. Young's modulus, Poisson's ration, water volume
 266 fraction, fibrillar direction and permeability) was developed under prolonged indentation tests. Other
 267 three material models (Models 2 to 4) were constructed to evaluate the effect of inhomogeneous material
 268 properties on the biomechanics of cartilage.

269 The predictions show that the fibril-reinforced biphasic mechanical properties and boundary

270 conditions adopted in the models are reasonable. Firstly, the creep displacement of Model 1 (9 layers;
271 strain-dependent) agrees with the previous study's data well. The 0.35 N force led to a slight deformation
272 of the cartilage, so the permeability which is strain-dependent would be altered slightly. Therefore, the
273 creep displacements of Model 1 and Model 4 (9 layers; constant) almost reached equilibrium at the same
274 time. Secondly, the fluid pressure distribution pattern is similar to the results of other finite element
275 studies under indentation tests [28]. The peak fluid support ratio of Model 1 is in accordant with those of
276 other models', such as the hip contact model [46] and the simplified patellar joint contact model [43].
277 Thirdly, as shown in Figure 7, the fluid only 'squeezed out' from the upper and lateral surface of the
278 cartilage and no fluid flux was allowed at the bottom surface [19], which is consistent with the boundary
279 condition suggested in this study.

280 The less than 3% difference in peak effective stress, contact pressure, fluid pressure as well as fluid
281 support ratio between Models 1 (9 layers; strain-dependent) and 2 (3 layers; strain-dependent) suggests
282 that it is feasible to construct the highly inhomogeneous properties of cartilage using a three-layered
283 model if these peak values are the outputs of interest (Figure 4, 5 and 9). However, as for the results of
284 Model 3 (1 layer; strain-dependent), up to 15% difference could be observed in the peak effective stress
285 when compared with that of Model 1. Effective stress and contact pressure were analysed, because they
286 were used as potential mechanical criteria for AC damage in many studies [20, 21]. In addition, 90% fluid
287 support ratios are shown in both Models 1 and 2, which highlights the important role that fluid

288 pressurisation and fluid support play in AC [43, 46]. This fluid support mechanism would prevent
289 over-loading to the solid-matrix, and at the same time, provide a low coefficient of friction, which is
290 essential to maintain the function of the cartilage [47]. However, the peak fluid support ratio was only
291 82% in Model 3, in which the fluid support ratio may be underestimated [21, 25, 33]. Thus, these results
292 may suggest that the application of over-simplified model (Mode 3) should be carefully evaluated.

293 The different stress and strain distribution pattern along depth in Model 1 to Model 3 in long-term
294 simulation may provide an important insight into the highly inhomogeneous properties of cartilage. As
295 shown in Figure 8, the effective stress and z-strain of Model 1 to Model 3 are similar under short-term
296 loading, but become different under long-term loading, suggesting that the load-bearing mechanism is
297 provided by the fluid phase under short-term loading and by the solid-matrix under long-term loading.
298 During short-term loading, the fluid within AC has no time to flow out due to the low permeability and
299 thus fluid support ratio is high. When the load is kept constant for a long time, the fluid support ratio
300 would decrease to nearly zero and the load would be transferred to the solid-matrix gradually. To sum up,
301 the different representation of the solid-matrix would cause a different stress and strain distribution
302 pattern along depth in long-term simulation, and more accurate representation of depth-dependent
303 properties could help to further access the simulation results such as stress and strain along depth of AC
304 [25].

305 Furthermore, this study suggests that accurate predictions of stress and strain through the thickness

306 could help to understand the interaction between chondrocytes and tissue. Previous studies shows that the
307 local high stress and strain within AC might cause death of the chondrocyte which would further lead to
308 tissue fibrillation or delamination [22, 23], as chondrocytes are shown to be important in protein synthesis
309 and metabolic activity [48]. Therefore, the accurate predictions of stress and strain along depth could help
310 to understand the role of mechanics on chondrocytes. Moreover, improving the resolution of the
311 simulation results such as stress and strain can also contribute markedly to optimization of the
312 depth-dependent scaffold structure in tissue-engineering. Because the proper stress and strain of scaffold
313 structure could help the chondrocytes to proliferate and migrate [3]. In the future, the highly
314 inhomogeneous depth-dependent properties could be adopted in a multiscale model considering
315 anatomical cell distribution [8] to understand the interaction between chondrocytes and cartilage, or in
316 tissue-engineering to reduce the biological tests by optimizing the depth-dependent scaffold structure [3,
317 4].

318 The strain-dependent permeability had a great effect on the mechanical behaviour of cartilage under
319 large deformation situation. Firstly, the permeability and the fluid flux of AC would decrease. In our study,
320 permeability decreased dramatically to about 20% of the initial value in the surface zone of Model 1 (9
321 layers; strain-dependent) (Figure 6). The peak total fluid flux under the indenter in Model 1 was almost
322 two thirds of the fluid flux in Model 4 (9 layers; constant permeability) in Figure 10(a). The decreasing
323 fluid flux could be caused by the decreasing permeability due to the large deformation of cartilage, which

324 has been observed in other experiments [15, 42]. Secondly, the time to reach the equilibrium state would
325 become longer. Because of the decrease of the fluid flux in Model 1, the fluid pressure of Model 1
326 reached equilibrium state more slowly (about 400 s) than Model 4 in Figure 10(b), which suggests that
327 the time to reach equilibrium state is influenced by the permeability of the articular cartilage [49]. Thirdly,
328 the fluid support ratio would decrease more slowly over time. The fluid support ratio of Model 1
329 decreased slower when compared with the fluid support ratio of Model 4 (Figure 10(d)). This result
330 highlights the positive effect of strain-dependent permeability on fluid pressurisation and the load support
331 capability. In addition, investigating the fluid diffusion mechanism within AC is also vital for the
332 biosynthesis of chondrocytes in AC and in scaffold model. Because AC as well as the scaffold model are
333 avascular, the ions and nutrients are transported by fluid diffusion [4, 16, 37]. Therefore, this study
334 suggests that the strain-dependent permeability would have a great effect on the biomechanical behaviour
335 of AC [42].

336 According to previous studies [10, 25, 50], both the material properties and number of elements of
337 the model were thought to be the key factors of the computational cost. However, in the present study, the
338 computational time in Model 1 was almost the same with the time cost of simplified models, which
339 indicated that the application of inhomogeneous material properties has limited influence on the
340 computational period under the same meshing condition. This finding has not been discussed before.
341 Although adopting complex material model would not add much computational cost in this study,

342 constructing and verifying such a highly inhomogeneous cartilage model in a real joint geometry is
343 always challenging. First, it is impossible to obtain all the detail in depth-dependent properties through
344 only one experiment and thus various experiments should be carried out on a great number of samples.
345 Then, due to measurement errors, the constructed model would need to be verified by experimental
346 results derived from the indentation or unconfined compression tests etc. Last but not the least, due to the
347 complexity of multi-layered fibril-reinforced biphasic cartilage in the joint, researchers may spend more
348 time to construct it. For example, it might be difficult to segment the cartilage into a multi-layered mesh
349 model due to the complex geometry of cartilage. It is also time-consuming to adjust the mesh of the
350 model as well as the nodal order of the elements which are needed to apply the desired fibrillar
351 distribution pattern to the cartilage model.

352 The present study has some limitations. Firstly, due to the difficulty of measuring the anisotropic
353 permeability [51], we assumed the permeability along the direction parallel to the fibres was twice as
354 much as that along the direction perpendicular to the fibres based on a previous study [25]. New method
355 and apparatus are needed to be developed in order to measure the permeability along all the three
356 orthogonal direction in the future [51]. Secondly, more realistic fibrillar distribution pattern that can be
357 measured using diffusion tensor magnetic resonance imaging was not adopted, which was used and tested
358 in our previous study indicating the application of the realistic orientation of fibre on a simple rectangle
359 model could predict more accurate mechanical information [21]. However, this study focused on the

360 influence of the depth-dependent and strain-dependent properties of the non-fibrillar matrix on the
361 biomechanics of cartilage. Therefore, the adopted fibrillar distribution pattern was adequate to discuss the
362 importance of the highly inhomogeneous properties. Thirdly, only one indentation model was considered,
363 and the predicted results may be influenced by more complex geometries such as a real joint model.
364 These limitations will be further addressed in future studies.

365 **5. Conclusion**

366 A highly inhomogeneous fibril-reinforced biphasic model considering both depth-dependent and
367 strain-dependent properties was developed in this study. The results provide important insights into the
368 effect of highly inhomogeneous properties on the mechanical behaviour of AC. As for the
369 depth-dependent properties, the choice of different multi-layered models should depend on the research
370 question and clinical demands. The three-layered and nine-layered models provided similar results
371 including the peak effective stress, contact pressure, fluid pressure as well as fluid support ratio. However,
372 the nine-layered model might be more suitable if detail information such as stress and strain along depth
373 within AC are needed over long-term loading. The choice of single-layered model should be cautiously
374 evaluated, as this model may not describe the mechanical behaviour as highly inhomogeneous model did.
375 In addition, the strain-dependent permeability was shown to have a great effect on the mechanical
376 behaviour of cartilage and an enhanced fluid pressurisation could be observed. Therefore, the present
377 study suggests that the highly inhomogeneous fibril-reinforced biphasic model shows different

378 biomechanics of AC compared with the simplified models. In future studies, the proposed model could be
379 adopted in multiscale models considering anatomical cell distribution within AC to provide more in-depth
380 information or in tissue-engineering to reduce the biological tests by optimizing the depth-dependent
381 scaffold structure.

382

383 **Funding**

384 This work was supported by National Natural Science Foundation of China [11902048, 51323007],
385 Natural Science Foundation of Shaanxi Province of China [2019JQ-243].

386 **Acknowledgements**

387 The authors would like to express gratitude to the FEBio developers.

388 **Conflicts of Interest**

389 None.

390

391

392

393

394 **References**

395 [1] V.C. Mow, X.E. Guo, Mechano-electrochemical properties of articular cartilage: their inhomogeneities

396 and anisotropies, *Annu Rev Biomed Eng*, 4 (2002) 175-209, doi:
397 10.1146/annurev.bioeng.4.110701.120309.

398 [2] S.S. Sajjadinia, M. Haghpanahi, M. Razi, Computational simulation of the multiphasic degeneration
399 of the bone-cartilage unit during osteoarthritis via indentation and unconfined compression tests, *Proc Inst*
400 *Mech Eng H*, 233 (2019) 871-882, doi: 10.1177/0954411919854011.

401 [3] C.R. Hassan, Y.X. Qin, D.E. Komatsu, S.M.Z. Uddin, Utilization of Finite Element Analysis for
402 Articular Cartilage Tissue Engineering, *Materials* (Basel, Switzerland), 12 (2019), doi:
403 10.3390/ma12203331.

404 [4] A.R. Farooqi, J. Zimmermann, R. Bader, U. van Rienen, Computational study on electromechanics of
405 electroactive hydrogels for cartilage-tissue repair, *Comput Methods Programs Biomed*, 197 (2020)
406 105739, doi: 10.1016/j.cmpb.2020.105739.

407 [5] A.A. Goldsmith, A. Hayes, S.E. Clift, Application of finite elements to the stress analysis of articular
408 cartilage, *Med Eng Phys*, 18 (1996) 89-98, doi: 10.1016/1350-4533(95)00029-1.

409 [6] V.C. Mow, S.C. Kuei, W.M. Lai, C.G. Armstrong, Biphasic creep and stress relaxation of articular
410 cartilage in compression? Theory and experiments, *J Biomech Eng*, 102 (1980) 73-84, doi:
411 10.1115/1.3138202.

412 [7] A. Komeili, A. Rasoulian, R. Kakavand, Effect of collagen fibril distributions on the crack profile in
413 articular cartilage, *Comput Methods Programs Biomed*, 195 (2020) 105648, doi:
414 10.1016/j.cmpb.2020.105648.

415 [8] P. Tanska, M.S. Venalainen, A. Erdemir, R.K. Korhonen, A multiscale framework for evaluating
416 three-dimensional cell mechanics in fibril-reinforced poroelastic tissues with anatomical cell distribution -
417 Analysis of chondrocyte deformation behavior in mechanically loaded articular cartilage, *J Biomech*, 101
418 (2020) 109648, doi: 10.1016/j.jbiomech.2020.109648.

419 [9] S.S. Sajjadinia, B. Carpentieri, G.A. Holzapfel, A backward pre-stressing algorithm for efficient finite
420 element implementation of in vivo material and geometrical parameters into fibril-reinforced mixture
421 models of articular cartilage, *J Mech Behav Biomed Mater*, 114 (2021) 104203, doi:
422 10.1016/j.jmbbm.2020.104203.

423 [10] O. Klets, M.E. Mononen, P. Tanska, M.T. Nieminen, R.K. Korhonen, S. Saarakkala, Comparison of
424 different material models of articular cartilage in 3D computational modeling of the knee: Data from the
425 Osteoarthritis Initiative (OAI), *J Biomech*, 49 (2016) 3891-3900, doi: 10.1016/j.jbiomech.2016.10.025.

426 [11] W.M. Lai, V.C. Mow, V. Roth, Effects of nonlinear strain-dependent permeability and rate of
427 compression on the stress behavior of articular cartilage, *J Biomech Eng*, 103 (1981) 61-66, doi:
428 10.1115/1.3138261.

429 [12] R.M. Schinagl, D. Gurskis, A.C. Chen, R.L. Sah, Depth-dependent confined compression modulus of
430 full-thickness bovine articular cartilage, *J Orthop Res*, 15 (1997) 499-506, doi: 10.1002/jor.1100150404.

- 431 [13] L.P. Li, M.D. Buschmann, A. Shirazi-Adl, A fibril reinforced nonhomogeneous poroelastic model for
432 articular cartilage: inhomogeneous response in unconfined compression, *J Biomech*, 33 (2000) 1533-1541,
433 doi: 10.1016/s0021-9290(00)00153-6.
- 434 [14] V.C. Mow, A. Ratcliffe, A.R. Poole, Cartilage and diarthrodial joints as paradigms for hierarchical
435 materials and structures, *Biomaterials*, 13 (1992) 67-97, doi: 10.1016/0142-9612(92)90001-5.
- 436 [15] M.H. Holmes, V.C. Mow, The nonlinear characteristics of soft gels and hydrated connective tissues
437 in ultrafiltration, *J Biomech*, 23 (1990) 1145-1156, doi: 10.1016/0021-9290(90)90007-p.
- 438 [16] M. Maleki, K. Hashlamoun, W. Herzog, S. Federico, Effect of structural distortions on articular
439 cartilage permeability under large deformations, *Biomech Model Mechanobiol*, 19 (2020) 317-334, doi:
440 10.1007/s10237-019-01213-6.
- 441 [17] G.A. Ateshian, J.A. Weiss, Anisotropic hydraulic permeability under finite deformation, *J Biomech*
442 *Eng*, 132 (2010) 111004, doi: 10.1115/1.4002588.
- 443 [18] K.B. Gu, L.P. Li, A human knee joint model considering fluid pressure and fiber orientation in
444 cartilages and menisci, *Med Eng Phys*, 33 (2011) 497-503, doi: 10.1016/j.medengphy.2010.12.001.
- 445 [19] A. Maroudas, P. Bullough, The Permeability of Articular Cartilage, *Nature*, 219 (1968) 1260-1261,
446 doi: 10.1302/0301-620X.50B1.166.
- 447 [20] J. Li, X. Hua, A.C. Jones, S. Williams, Z. Jin, J. Fisher, R.K. Wilcox, The influence of the
448 representation of collagen fibre organisation on the cartilage contact mechanics of the hip joint, *J*
449 *Biomech*, 49 (2016) 1679-1685, doi: 10.1016/j.jbiomech.2016.03.050.
- 450 [21] Q. Meng, S. An, R.A. Damion, Z. Jin, R. Wilcox, J. Fisher, A. Jones, The effect of collagen fibril
451 orientation on the biphasic mechanics of articular cartilage, *J Mech Behav Biomed Mater*, 65 (2017)
452 439-453, doi: 10.1016/j.jmbbm.2016.09.001.
- 453 [22] S. Chegini, S.J. Ferguson, Time and depth dependent Poisson's ratio of cartilage explained by an
454 inhomogeneous orthotropic fiber embedded biphasic model, *J Biomech*, 43 (2010) 1660-1666, doi:
455 10.1016/j.jbiomech.2010.03.006.
- 456 [23] W. Huang, M. Warner, H. Sasaki, K.S. Furukawa, T. Ushida, Layer dependence in strain distribution
457 and chondrocyte damage in porcine articular cartilage exposed to excessive compressive stress loading, *J*
458 *Mech Behav Biomed Mater*, 112 (2020) 104088, doi: 10.1016/j.jmbbm.2020.104088.
- 459 [24] S. Manzano, M. Armengol, J.P. A, A.H. P, S.G. H, M. Doblare, M. Hamdy Doweidar,
460 Inhomogeneous Response of Articular Cartilage: A Three-Dimensional Multiphasic Heterogeneous Study,
461 *PLoS One*, 11 (2016) e0157967, doi: 10.1371/journal.pone.0157967.
- 462 [25] Y. Dabiri, L.P. Li, Influences of the depth-dependent material inhomogeneity of articular cartilage on
463 the fluid pressurization in the human knee, *Med Eng Phys*, 35 (2013) 1591-1598, doi:
464 10.1016/j.medengphy.2013.05.005.
- 465 [26] H. Guo, R.L. Spilker, An augmented Lagrangian finite element formulation for 3D contact of

466 biphasic tissues, *Comput Methods Biomech Biomed Engin*, 17 (2014) 1206-1216, doi:
467 10.1080/10255842.2012.739166.

468 [27] J. Li, T.D. Stewart, Z. Jin, R.K. Wilcox, J. Fisher, The influence of size, clearance, cartilage
469 properties, thickness and hemiarthroplasty on the contact mechanics of the hip joint with biphasic layers,
470 *J Biomech*, 46 (2013) 1641-1647, doi: 10.1016/j.jbiomech.2013.04.009.

471 [28] Q. Meng, Z. Jin, J. Fisher, R. Wilcox, Comparison between FEBio and Abaqus for biphasic contact
472 problems, *Proc Inst Mech Eng H*, 227 (2013) 1009-1019, doi: 10.1177/0954411913483537.

473 [29] R.L. Spilker, J.K. Suh, V.C. Mow, A finite element analysis of the indentation stress-relaxation
474 response of linear biphasic articular cartilage, *J Biomech Eng*, 114 (1992) 191-201, doi:
475 10.1115/1.2891371.

476 [30] K.E. Keenan, L.C. Kourtis, T.F. Besier, D.P. Lindsey, G.E. Gold, S.L. Delp, G.S. Beaupre, New
477 resource for the computation of cartilage biphasic material properties with the interpolant response
478 surface method, *Comput Methods Biomech Biomed Engin*, 12 (2009) 415-422, doi:
479 10.1080/10255840802654319.

480 [31] Y. Li, E.H. Frank, Y. Wang, S. Chubinskaya, H.H. Huang, A.J. Grodzinsky, Moderate dynamic
481 compression inhibits pro-catabolic response of cartilage to mechanical injury, tumor necrosis factor-alpha
482 and interleukin-6, but accentuates degradation above a strain threshold, *Osteoarthritis Cartilage*, 21 (2013)
483 1933-1941, doi: 10.1016/j.joca.2013.08.021.

484 [32] R.M. Schinagl, M.K. Ting, J.H. Price, R.L. Sah, Video microscopy to quantitate the inhomogeneous
485 equilibrium strain within articular cartilage during confined compression, *Ann Biomed Eng*, 24 (1996)
486 500-512, doi: 10.1007/BF02648112.

487 [33] M.A. Soltz, G.A. Ateshian, Experimental verification and theoretical prediction of cartilage
488 interstitial fluid pressurization at an impermeable contact interface in confined compression, *J Biomech*,
489 31 (1998) 927-934, doi: 10.1016/S0021-9290(98)00105-5.

490 [34] D.M. Pierce, T. Ricken, G.A. Holzapfel, A hyperelastic biphasic fibre-reinforced model of articular
491 cartilage considering distributed collagen fibre orientations: continuum basis, computational aspects and
492 applications, *Comput Methods Biomech Biomed Engin*, 16 (2013) 1344-1361, doi:
493 10.1080/10255842.2012.670854.

494 [35] L.A. Setton, H. Tohyama, V.C. Mow, Swelling and curling behaviors of articular cartilage, *J*
495 *Biomech Eng*, 120 (1998) 355-361, doi: 10.1115/1.2798002.

496 [36] L. Han, Eliot H. Frank, Jacqueline J. Greene, H.-Y. Lee, H.-Hwa K. Hung, Alan J. Grodzinsky, C.
497 Ortiz, Time-Dependent Nanomechanics of Cartilage, *Biophysical Journal*, 100 (2011) 1846-1854, doi:
498 10.1016/j.bpj.2011.02.031.

499 [37] J.A. Wahlquist, C.M. Heveran, C.P. Neu, V.L. Ferguson, F.W. DelRio, M.A. Randolph, A.H. Aziz,
500 S.J. Bryant, Indentation mapping revealed poroelastic, but not viscoelastic, properties spanning native

501 zonal articular cartilage, *Acta Biomaterialia*, 64 (2017) 41-49, doi: 10.1016/j.actbio.2017.10.003.
502 [38] E.B. Hunziker, M. Michel, D. Studer, Ultrastructure of adult human articular cartilage matrix after
503 cryotechnical processing, *Microsc Res Tech*, 37 (1997) 271-284, doi:
504 10.1002/(SICI)1097-0029(19970515)37:4<271::AID-JEMT3>3.0.CO;2-O.
505 [39] G.A. Ateshian, V. Rajan, N.O. Chahine, C.E. Canal, C.T. Hung, Modeling the matrix of articular
506 cartilage using a continuous fiber angular distribution predicts many observed phenomena, *J Biomech*
507 *Eng*, 131 (2009) 061003, doi: 10.1115/1.3118773.
508 [40] S. Maas, D. Rawlins, J.A. Weiss, G.A. Ateshian, *FEBio Theory Manual – Version 2.9*, University of
509 Utah, Salt Lake City, Utah.2019.
510 [41] E.M. Shapiro, A. Borthakur, J.H. Kaufman, J.S. Leigh, R. Reddy, Water distribution patterns inside
511 bovine articular cartilage as visualized by 1H magnetic resonance imaging, *Osteoarthritis Cartilage*, 9
512 (2001) 533-538, doi: 10.1053/joca.2001.0428.
513 [42] W.M. Lai, V.C. Mow, Drag-induced compression of articular cartilage during a permeation
514 experiment, *Biorheology*, 17 (1980) 111-123, doi: 10.3233/bir-1980-171-213.
515 [43] R. Krishnan, S. Park, F. Eckstein, G.A. Ateshian, Inhomogeneous cartilage properties enhance
516 superficial interstitial fluid support and frictional properties, but do not provide a homogeneous state of
517 stress, *J Biomech Eng*, 125 (2003) 569-577, doi: 10.1115/1.1610018.
518 [44] S.A. Maas, B.J. Ellis, G.A. Ateshian, J.A. Weiss, *FEBio: finite elements for biomechanics*, *J Biomech*
519 *Eng*, 134 (2012) 011005, doi: 10.1115/1.4005694.
520 [45] G.A. Ateshian, S. Maas, J.A. Weiss, Finite element algorithm for frictionless contact of porous
521 permeable media under finite deformation and sliding, *J Biomech Eng*, 132 (2010) 061006, doi:
522 10.1115/1.4001034.
523 [46] J. Li, X. Hua, Z. Jin, J. Fisher, R.K. Wilcox, Biphasic investigation of contact mechanics in natural
524 human hips during activities, *Proc Inst Mech Eng H*, 228 (2014) 556-563, doi:
525 10.1177/0954411914537617.
526 [47] L.A. Setton, W. Zhu, V.C. Mow, The biphasic poroviscoelastic behavior of articular cartilage: role of
527 the surface zone in governing the compressive behavior, *J Biomech*, 26 (1993) 581-592, doi:
528 10.1016/0021-9290(93)90019-b.
529 [48] J.Y. Shyy, S. Chien, Role of integrins in cellular responses to mechanical stress and adhesion, *Curr*
530 *Opin Cell Biol*, 9 (1997) 707-713, doi: 10.1016/s0955-0674(97)80125-1.
531 [49] C.G. Armstrong, V.C. Mow, Variations in the intrinsic mechanical properties of human articular
532 cartilage with age, degeneration, and water content, *J Bone Joint Surg Am*, 64 (1982) 88-94, doi:
533 10.2106/00004623-198264010-00013.
534 [50] L.P. Li, K.B. Gu, Reconsideration on the use of elastic models to predict the instantaneous load
535 response of the knee joint, *Proc Inst Mech Eng H*, 225 (2011) 888-896, doi: 10.1177/0954411911412464.

536 [51] A. Tomic, A. Grillo, S. Federico, Poroelastic materials reinforced by statistically oriented
537 fibres--numerical implementation and application to articular cartilage, *IMA Journal of Applied*
538 *Mathematics*, 79 (2014) 1027-1059, doi: 10.1093/imamat/hxu039.
539